Journal of Applied Mechanics and Technical Physics, Vol. 42, No. 6, pp. 1014–1022, 2001

ADJOINT PROBLEMS OF MECHANICS OF CONTINUOUS MEDIA IN GAS-LASER CUTTING OF METALS

O. B. Kovalev, A. M. Orishich, V. M. Fomin, and V. B. Shulyat'ev

UDC 621.373.826

A mathematical model of gas-laser cutting of metal plates in an inert gas is proposed. The formation and flow of the liquid metal melt film at the cutting front is considered within the framework of incompressible boundary-layer equations. Based on the resultant analytical solution, a local law of energy conservation on the cutting surface is derived, which takes into account the melt-film thickness and the temperature dependence of thermophysical parameters of the metal. The problem of the cutting shape and depth is solved in the two-dimensional formulation. A comparison with experimental data is made in terms of the cutting depth and maximum cutting velocity for carbon and alloy steel.

Introduction. Rapid development of laser methods of metal processing is caused by the high level of technological parameters, such as accuracy, locality of action, and velocity and quality of processing. Most metals exhibit good absorption of radiation from a focused laser beam. Absorption of laser radiation by metals is accompanied by various physicochemical processes, such as heating, melting, evaporation, oxidation, and removal of the melt. In the radiation spot, a material may be rapidly heated, melt, and even evaporate. Laser energy is absorbed by the surface layer of the metal and propagates due to heat conduction in the axial and radial directions. If the power density of the incident radiation is small (less than 10^8 W/m^2) and the absorption rate is small as compared to heat removal, then the surface temperature in the radiation spot is lower than the melting point. For a high power density (greater than 10^{10} W/m^2), evaporation becomes a dominant mechanism of material removal. Note that all processes are rather localized because of the small size of the radiation spot (about 10^{-4} m).

Gas-laser cutting (GLC) of metals is widely used in fabrication of machine elements. The possibility of using GLC depends significantly on the quality of cutting (roughness, burrs, cutting-zone geometry, etc.). GLC includes many interrelated physical processes and is performed by means of local melting of the metal and removal of the melt by the gas flow. GLC is an economical process that does not require a high laser power, since the melting heat for metals is much lower than the evaporation heat. The use of an oxidizing gas (air or oxygen) leads to chemical reactions with additional heat release in the surface layer, which also allows reduction of the laser power. As the laser beam moves along the surface of a metal plate, a cutting kerf is formed. At the cutting front subjected to the action of the gas jet and radiation, the melted metal flows in the form of a liquid film. The cutting depth and purity (roughness) depend on a large number of parameters, which are difficult to predict. For example, one possible reason for the formation of burrs and ripple patterns on the cutting edges is the unstable nonstationary motion of the liquid film.

With increasing requirements to the quality of articles produced by laser technologies, it becomes necessary to describe more accurately the inherent physicochemical processes. Nevertheless, despite the large number of papers in this field [1–8], there is no adequate description of the processes typical of GLC of metals.

Institute of Theoretical and Applied Mechanics, Siberian Division, Russian Academy of Sciences, Novosibirsk 630090. Translated from Prikladnaya Mekhanika i Tekhnicheskaya Fizika, Vol. 42, No. 6, pp. 106–116, November–December, 2001. Original article submitted May 28, 2001.

 0021-8944/01/4206-1014 $25.00

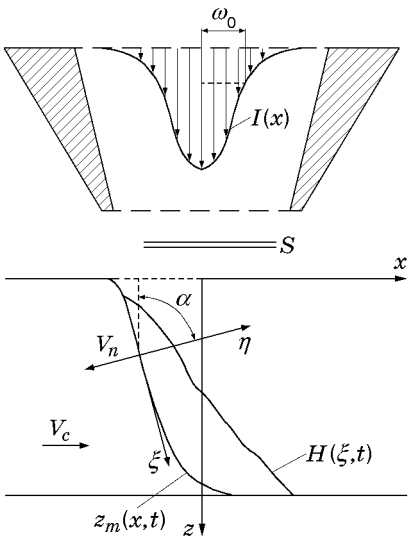

Fig. 1. Interaction of the laser beam and gas jet with the surface of the metal plate and melt layer.

To describe a realistic GLC pattern, it is necessary to consider a number of adjoint problems of mechanics of continuous media:

— exhaustion of a gas jet and its dynamic interaction with the melted metal are described by the gas-dynamics equations or Navier–Stokes equations;

— heat propagation in the solid body and melting of the metal are described by the heat-conduction equations and two-phase Stefan problem;

— thermal interaction of laser radiation with the surface, the formation of the metal melt, and its flow in the form of a liquid film are described by the incompressible boundary-layer equations.

The solution of the above equations in the full-scale formulation seems to be rather problematic. Therefore, in the approach proposed in the present paper, the generic formulation of the GLC problem is separated in terms of physical processes into subproblems; each subproblem is solved analytically under certain assumptions.

Gas Jet. The scheme of interaction of the laser beam and gas jet with the surface of a metal plate is shown in Fig. 1 (S is the normal shock). The coordinate system (x, z) is rigidly fitted to the beam axis. A jet of an inert gas is injected parallel to the laser beam. The velocity, density, and pressure of the inert gas do not change with time. The formulation and solution of the problem of interaction of a supersonic gas jet and a plate with a cutting kerf is severely complicated by the presence of a channel-slotted jet flow with turbulent boundary layers and a system of shock waves [4]. Therefore, we consider a simplified one-dimensional formulation of the problem, where the nozzle-exit diameter is much larger than the cutting width. The gas-dynamic parameters of the jet are constant in each cross section of the cutting kerf aligned perpendicular to the jet direction. If the pressure in the gas holder P_0 is known and the ambient pressure P_a is specified, then the gas parameters at the nozzle exit are calculated by the following isentropic formulas [9]:

$$P_1 = P_0\Big(1 - \frac{k_\mathrm{g}-1}{k_\mathrm{g}+1}\,\lambda_1^2\Big)^{k_\mathrm{g}/(k_\mathrm{g}-1)}, \quad \rho_1 = \rho_0\Big(1 - \frac{k_\mathrm{g}-1}{k_\mathrm{g}+1}\,\lambda_1^2\Big)^{1/(k_\mathrm{g}-1)}, \quad T_1 = T_0\Big(1 - \frac{k_\mathrm{g}-1}{k_\mathrm{g}+1}\,\lambda_1^2\Big),$$

$$\lambda_1^2 = \frac{k_\mathrm{g}+1}{k_\mathrm{g}-1}\Big(1 - \Big(\frac{P_\mathrm{a}}{P_0}\Big)^{(k_\mathrm{g}-1)/k_\mathrm{g}}\Big), \quad V_1 = \lambda_1 a_\mathrm{c}, \quad a_\mathrm{c} = \sqrt{\frac{2k_\mathrm{g}}{k_\mathrm{g}+1}\,R_\mathrm{g}T_*}. \tag{1}$$

Here P_1, ρ_1, T_1, and V_1 are the gas pressure, density, temperature, and velocity at the nozzle exit, k_g and R_g are the ratio of specific heats and the gas constant, λ_1 is the reduced velocity, a_cr is the critical velocity of sound, and T_* is the stagnation temperature.

In the case of supersonic exhaustion ($\lambda_1 > 1$), a normal shock wave arises between the nozzle and the plate. The parameters behind this shock are calculated by the formulas

$$\lambda_2 = \frac{1}{\lambda_1}, \quad P_2 = P_1 \frac{\lambda_1^2 - (k_\mathrm{g}-1)/(k_\mathrm{g}+1)}{1 - \lambda_1^2(k_\mathrm{g}-1)/(k_\mathrm{g}+1)}, \quad \rho_2 = \rho_1 \lambda_1^2, \quad T_2 = \frac{P_2}{\rho_2 R_\mathrm{g}}. \tag{2}$$

In describing the gas motion in a slot, we assume that the pressure gradient $dP/d\xi$ is a constant quantity, which can be evaluated from the Bernoulli equation $k = -dP/d\xi \approx \Delta P/L = 0.5\rho_2 V_2^2/L$ (L is the thickness of the metal plate and ξ is the coordinate fitted to the cut-front surface). Taking into account the continuity equation for the gas $\rho V_\mathrm{g} = \rho_2 V_2 = \mathrm{const}$, we obtain

$$P = P_2 - 0.5\rho_2 V_2^2 \xi/L, \quad V_\mathrm{g} = V_2(1 + 0.5\xi/L), \quad \rho = \rho_2/(1 + 0.5\xi/L), \quad T_\mathrm{g} = P/(\rho R_\mathrm{g}). \tag{3}$$

Thus, the gas pressure P, velocity V_g, density ρ, and temperature T_g in the slot are calculated using formulas (1)–(3).

Laser Radiation. We consider radiation of a CO_2 laser with a 10.6-μm wavelength. The intensity of the laser beam is described by the Gaussian distribution $I(r) = I_0 \exp(-2r^2/\omega_0^2)$, where $I_0 = 2W/(\pi\omega_0^2)$, $r = \sqrt{x^2 + y^2}$, W is the laser power, and ω_0 is the beam radius. Radiation absorption depends on the reflectance of the metal surface. The description of radiation/metal interaction involves Fresnel's equations from which it follows that the reflectivity is related to the complex refractive index of workpiece $N = n_\omega + ik_\omega$ (n_ω and k_ω are the refractive index and the extinction index of the medium) and the angle of incidence of the beam γ and depends on radiation polarization, which may be parallel (R_s) or perpendicular (R_p) to the plane of incidence [10]:

$$R_s = \Big|\frac{\cos\gamma - (N^2 - \sin^2\gamma)^{1/2}}{\cos\gamma + (N^2 - \sin^2\gamma)^{1/2}}\Big|^2, \quad R_p = \Big|\frac{N^2\cos\gamma - (N^2 - \sin^2\gamma)^{1/2}}{N^2\cos\gamma + (N^2 - \sin^2\gamma)^{1/2}}\Big|^2.$$

In the case of circular polarization, where the direction of the vector of electric-field intensity changes periodically from parallel to perpendicular, the absorption factor is calculated by the formula $A(\gamma) = 1 - 0.5(R_s + R_p)$.

Flow of a Liquid Film. The motion of the melt film is considered in the coordinate system (ξ, η) fitted to the cutting-front surface $z = z_\mathrm{m}(x)$ (Fig. 1) as follows:

$$\xi = (x + \omega_0)\cos\alpha + z\sin\alpha, \qquad \eta = (x + \omega_0)\sin\alpha - z\cos\alpha; \tag{4}$$

$$\cos\alpha = 1\Big/\sqrt{1 + (z_\mathrm{m})_x'^2}. \tag{5}$$

Under GLC conditions, it is usually assumed that the thickness of the down-flowing film is much smaller than the cutting width [4]. The action of mass forces on the liquid may be ignored, and the melt flow may be described by incompressible boundary-layer equations [3, 11]

$$\frac{\partial U}{\partial \xi} + \frac{\partial V}{\partial \eta} = 0; \tag{6}$$

$$\rho_\mathrm{m}\Big(\frac{\partial U}{\partial t} + U\frac{\partial U}{\partial \xi} + V\frac{\partial U}{\partial \eta}\Big) = -\frac{dP}{d\xi} + \mu_\mathrm{m}\frac{\partial^2 U}{\partial \eta^2}; \tag{7}$$

$$\rho_\mathrm{m}\Big(\frac{\partial E}{\partial t} + U\frac{\partial E}{\partial \xi} + V\frac{\partial E}{\partial \eta}\Big) = U\frac{dP}{d\xi} + \frac{\partial}{\partial \eta}\Big(\rho_\mathrm{m} æ_\mathrm{m}\frac{\partial E}{\partial \eta}\Big) + \mu_\mathrm{m}\Big(\frac{\partial U}{\partial \eta}\Big)^2. \tag{8}$$

Here U and V are the velocity-vector components in the ξ and η directions, respectively, $E = c_\mathrm{m}T$ (T is the temperature), ρ_m, c_m, and μ_m are the density, specific heat capacity, and viscosity of the liquid metal, and $æ_\mathrm{m} = \lambda_\mathrm{m}/(\rho_\mathrm{m}c_\mathrm{m})$ is the temperature diffusivity.

We set the boundary conditions for Eqs. (6)–(8). The moving boundary $\eta = 0$, where metal melting occurs, moves along the normal to the cutting-front surface with a velocity V_n. The continuity conditions for velocity components of the liquid

$$\eta = 0: \qquad U(\xi, 0) = V_\mathrm{c}\cos\alpha, \quad V(\xi, 0) = V_\mathrm{c}\sin\alpha \tag{9}$$

and the Stefan conditions

$$\eta = 0: \qquad \lambda_\mathrm{m}\frac{\partial T}{\partial \eta} - \lambda_s\frac{\partial T_s}{\partial \eta} = \rho_\mathrm{m}H_\mathrm{m}V_\mathrm{n}, \quad T(\xi, 0) = T_s(\xi, 0) = T_\mathrm{m} \tag{10}$$

are satisfied at this boundary. Here λ_m and λ_s are the thermal conductivities of the melted and solid metal, T_s is the temperature of the solid metal, T_m and H_m are the melting point and latent heat of the metal, V_c is the velocity

of the plate motion relative to the laser beam or the cutting velocity, and $V_{\rm n}$ is the normal component of velocity vector of the liquid–solid interface.

At the other moving boundary $\eta = H(\xi, t)$ (H is the thickness of the liquid melt layer), which is the liquid–gas interface, the condition that describes the dynamic interaction between the gas and the liquid

$$\eta = H(\xi, t): \qquad \mu_{\rm m} \frac{\partial U}{\partial \eta} = \tau \tag{11}$$

(τ is the tangential stress at the liquid–gas interface) and the condition of kinematic compatibility

$$\eta = H(\xi, t): \qquad \frac{\partial H}{\partial t} + U \frac{\partial H}{\partial \xi} = V \tag{12}$$

are satisfied. The following condition of interaction of laser radiation and the liquid surface (Fig. 1) is satisfied at the boundary $\eta = H(\xi, t)$:

$$\boldsymbol{q} \cdot \boldsymbol{n} = \lambda_{\rm m} \nabla T \cdot \boldsymbol{n}. \tag{13}$$

Here $\boldsymbol{n} = (-\sin\alpha, \cos\alpha)$.

In the (x, z) coordinates, the radiation-flux direction $\boldsymbol{q} = (0, q_z)$, where $q_z = (2A(\gamma)W/(\pi\omega_0^2)) \exp(-x^2/\omega_0^2)$, coincides with the Oz axis. According to Eqs. (4) and (5), we have $\boldsymbol{q} = (q_\xi, q_\eta) = (-q_z \sin\alpha, q_z \cos\alpha)$. Taking into account the assumption $\partial T/\partial\xi \approx 0$, from (13) we obtain

$$\eta = H(\xi, t): \qquad \lambda_{\rm m} \frac{\partial T}{\partial \eta} = \frac{2A(\gamma)W}{\pi\omega_0^2} \frac{\cos(\alpha - \varphi)}{\cos\varphi} \exp\Big(-\frac{2(\xi\cos\alpha + H(\xi)\sin\alpha - \omega_0)^2}{\omega_0^2}\Big). \tag{14}$$

Here γ is the angle of incidence of the beam onto the liquid surface and $A(\gamma)$ is the radiation-absorption factor, and

$$\cos\varphi = 1\Big/\sqrt{1 + H_\xi'^2}, \qquad \gamma = \alpha - \varphi. \tag{15}$$

Equations (6)–(15) describe the flow of a liquid film sustained by the force action of the gas. The equality of tangential stresses is fulfilled at the liquid–gas interface. According to the boundary-layer theory [11], we have $\tau = \sqrt{\mu_{\rm g}^* \rho_{\rm g}^* V_{\rm g}^3/L}$, where $\rho_{\rm g}^*$ and $\mu_{\rm g}^*$ are the gas density and viscosity at a temperature equal to the film-surface temperature. Nitrogen, which is considered as neutral in laser-cutting processes, was chosen as an assist gas [1].

Thermal Conductivity in Solids. It is known [4] that the scale of thermal conductivity of a material in the direction perpendicular to the optical axis of the beam is small as compared to the longitudinal scale, which is obviously valid for a thin plate. Since the velocity $V_{\rm n}$ of the phase-transition boundary is comparable in order of magnitude with the cutting velocity $V_{\rm c}$, the characteristic thickness of the heated layer of the material is $\Delta = æ_{\rm m}/V_{\rm n} \approx æ_{\rm m}/V_{\rm c} \approx 10^{-4}$ m. Therefore, heat propagation across the plate may be ignored. In addition to Eqs. (6)–(8), at each point ξ in the region $\eta \in (-\infty, 0)$, we consider the one-dimensional heat-conduction equation

$$\begin{gathered} c_s(T_s)\rho_s(T_s)\Big(\frac{\partial T_s}{\partial t} + V_{\rm n}\frac{\partial T_s}{\partial \eta}\Big) = \frac{\partial}{\partial \eta}\lambda_s(T_s)\frac{\partial T_s}{\partial \eta}, \\ \eta = 0: \quad T_s = T_{\rm m}, \qquad \eta = -\infty: \quad T_s = T_0. \end{gathered} \tag{16}$$

The thermophysical parameters of a material are temperature-dependent [12, 13]. As iron is heated from the normal temperature to its melting point, its density decreases by 0.5% [12], its heat capacity increases by 37% [13], and its thermal conductivity decreases by 45% with heating up to 1000 K and by another 10% with heating up to 1700 K [12]. At the phase-transition point, the thermophysical parameters also change: the iron density decreases by 7%, its heat capacity increases by 7%, and its thermal conductivity decreases from 39 W/(m·K) at 1400 K to 8–10 W/(m·K) [13]. Taking into account the above information, we use the values of thermophysical parameters listed in Table 1 and also the dependences of the parameters c_s [J/(kg·K)], ρ_s [kg/m^3], and λ_s [W/(m·K)] on the temperature T_s [7, 13, 14]:

$$c_s(T_s) = 477 + 0.233(T_s - T_0), \quad \rho_s(T_s) = 7900 - 0.73(T_s - T_0), \quad \lambda_s(T_s) = 47 - 0.024(T_s - T_0).$$

For given constant values of the thermophysical parameters of the melt $\rho_{\rm m}$, $c_{\rm m}$, $\mu_{\rm m}$, and $æ_{\rm m}$, radiation parameters $A(\gamma)$, W, and ω_0, pressure gradient in the gas k, and stress τ, Eqs. (6)–(16) yield the film thickness $H(\xi)$, the melting rate $V_{\rm n}$, and the flow parameters U, V, and T. For the beam motion with a velocity $V_{\rm c}$ relative to the stationary metal plate, the angle α depends on the cutting-front shape $z = z_{\rm m}(x, t)$ (Fig. 1). The relationship

TABLE 1

Material	T_{m}, K	H_{m}, kJ/kg	λ_s^0, W/(m·K)	λ_{m}, W/(m·K)	c_s^0, J/(kg·K)	c_{m}, J/(kg·K)	ρ_s^0, 10^3 kg/m^3	ρ_{m}, 10^3 kg/m^3	n_ω	k_ω	Reference
Fe	1808	277	39.0	10.0	628	748	7.8	6.98	7.60	27.0	[15]
St. 304	1670	—	—	31.5	707	810	7.9	6.90	6.02	—	[7]
St. 304	1800	275	14.9	—	477	—	7.9	—	17.87	28.5	[6]
Fe	1809	272	78.2	—	456	—	7.87	—	—	—	[8]
Fe	1810	276	40.0	9.0	700	—	7.8	—	4.20	12.6	[14, 15]

between the surface velocity V_{n} and the cutting velocity V_{c} is expressed by the equation of kinematic compatibility of the cutting-surface points:

$$\frac{\partial z_{\mathrm{m}}}{\partial t} - V_{\mathrm{c}}\frac{\partial z_{\mathrm{m}}}{\partial x} = -V_{\mathrm{n}}\sqrt{1+\Big(\frac{\partial z_{\mathrm{m}}}{\partial x}\Big)^2}. \tag{17}$$

Solution of Adjoint Problems. We assume that the action of laser radiation is continuous and the velocity of the plate relative to the beam is constant. Then the position of the cutting surface and also the liquid flow and temperature distribution in the solid may be assumed to be stationary. We obtain $V_{\mathrm{n}} = V_{\mathrm{c}}\sin\alpha$ from Eq. (17) in the stationary case. Ignoring convective terms in Eqs. (7) and (8), we write Eqs. (6)–(16) in the stationary dimensionless form:

$$\frac{\partial u}{\partial \xi'} + \frac{\partial v}{\partial \eta'} = 0, \qquad 0 \leqslant \eta' \leqslant h; \tag{18}$$

$$\frac{\partial^2 u}{\partial \eta'^2} = -AB; \tag{19}$$

$$\frac{\partial^2 \theta}{\partial \eta'^2} = \mathrm{Pe}\, v\frac{\partial \theta}{\partial \eta'} + C\mathrm{Pr}\Big(ABu - \Big(\frac{\partial u}{\partial \eta'}\Big)^2\Big); \tag{20}$$

$$\eta' = 0: \qquad u = \cos\alpha, \quad v = \sin\alpha, \quad \theta = 1; \tag{21}$$

$$\eta' = h(\xi'): \qquad \frac{\partial u}{\partial \eta'} = A, \quad v = 0, \quad u\frac{\partial h}{\partial \xi'} = v; \tag{22}$$

$$\eta' = h(\xi'): \qquad \frac{\partial \theta}{\partial \eta'} = \Omega A(\gamma)\frac{\cos(\alpha-\varphi)}{\cos\varphi}\exp\Big(-2(\xi'\cos\alpha + h(\xi')\sin\alpha - 1)^2\Big); \tag{23}$$

$$\begin{gathered}\frac{\partial}{\partial \eta'}\Big(\lambda(\theta_s)\frac{\partial \theta_s}{\partial \eta'}\Big) - æ\mathrm{Pe}\sin\alpha\nu(\theta_s)\frac{\partial \theta_s}{\partial \eta'} = 0, \qquad -\infty \leqslant \eta' \leqslant 0,\\ \lambda(\theta_s) = \lambda_s(\theta_s)/\lambda_s^0, \qquad \nu(\theta_s) = c_s(\theta_s)\rho_s(\theta_s)/(c_s^0\rho_s^0);\end{gathered} \tag{24}$$

$$\eta' = 0: \qquad \theta_s = 1; \tag{25}$$

$$\eta' = -\infty: \qquad \theta_s = 0, \quad \frac{\partial \theta_s}{\partial \eta'} = 0; \tag{26}$$

$$\eta' = 0: \qquad \frac{\partial \theta}{\partial \eta'} - \frac{\lambda_s^0}{\lambda_{\mathrm{m}}}\lambda(\theta_s)\frac{\partial \theta_s}{\partial \eta'} = \mathrm{Pe}\,\mathrm{Sf}\sin\alpha. \tag{27}$$

Here $\xi' = \xi/\omega_0$, $\eta' = \eta/\omega_0$, $h = H/\omega_0$, $u = U/V_{\mathrm{c}}$, $v = V/V_{\mathrm{c}}$, $\theta = (T-T_0)/(T_{\mathrm{m}}-T_0)$, $\theta_s = (T_s-T_0)/(T_{\mathrm{m}}-T_0)$, $A = \omega_0\tau/(\mu_{\mathrm{m}}V_{\mathrm{c}})$, $B = k\omega_0/\tau$, $C = V_{\mathrm{c}}^2/(c_{\mathrm{m}}(T_{\mathrm{m}}-T_0))$, $æ = æ_{\mathrm{m}}/æ_s^0$, $\mathrm{Pr} = \mu_{\mathrm{m}}/(\rho_{\mathrm{m}}æ_{\mathrm{m}})$ is the Prandtl number, $\mathrm{Pe} = (V_{\mathrm{c}}\omega_0)/æ_{\mathrm{m}}$ is the Peclet number, $\mathrm{Sf} = H_{\mathrm{m}}/(c_{\mathrm{m}}(T_{\mathrm{m}}-T_0))$ is the Stefan number, and $\Omega = 2W/(\pi\omega_0\lambda_{\mathrm{m}}(T_{\mathrm{m}}-T_0))$ is the degree of the energy action of radiation. The parameters A and B characterize the dynamics of the liquid, and the parameter C characterizes the effect of this dynamics on the temperature of the liquid.

Thus, the adjoint problems (18)–(27) admit integration with respect to the coordinate η' at each point ξ'. Integrating Eqs. (18) and (19), we obtain the distributions of the u and v components of the flow velocity

$$u = \cos\alpha + A(\eta' + B(h\eta' - 0.5\eta'^2)), \tag{28}$$

$$v = \sin\alpha - 0.5AB\,\frac{\partial h}{\partial \xi'}\,\eta'^2 \tag{29}$$

and the relation

$$(\xi' - \xi'_0)\sin\alpha = (h - h_0)\cos\alpha + A(h^2 - h_0^2)/2 + AB(h^3 - h_0^3)/3, \tag{30}$$

where h_0 is the film thickness in the beginning of the boundary layer ($\xi' = \xi'_0$).

Typical values of dimensionless parameters in the energy equation (20) are as follows: $\mathrm{Pr} = 10^{-2}$, $\mathrm{Pe} = 8$, $A = 10^3$, $B = 20$, and $C = 10^{-8}$. The power of laser radiation is $W = 600$ W, and the beam radius is $\omega_0 = 70$ μm. The estimates show that the effect of dynamics of the liquid on the changes in temperature across the melt layer is negligible; we may ignore this effect and assume that $C = 0$ in Eq. (20). Then, from the first integral in Eq. (20), we obtain the temperature-gradient distribution

$$\frac{\partial\theta}{\partial\eta'} = \Omega\mathrm{Pr}A(\gamma)\,\frac{\cos(\alpha - \varphi)}{\cos\varphi}\exp\Big(-2(\xi'\cos\alpha + h(\xi')\sin\alpha - 1)^2$$

$$+\,\mathrm{Pe}\sin\alpha\Big(\eta' - h - \frac{1}{6}\,\frac{AB(\eta'^3 - h^3)}{\cos\alpha + A(1 + Bh)h}\Big)\Big). \tag{31}$$

At the same time, the first integral in Eqs. (24)–(26) determines the heat flux in the solid:

$$\lambda(\theta_s)\,\frac{\partial\theta_s}{\partial\eta'} = æ\mathrm{Pe}\sin\alpha\int\limits_0^1 \nu(t)\,dt. \tag{32}$$

Substituting the expressions for heat fluxes into the Stefan condition (27), we obtain the relation between the angles α, φ, and γ and the liquid-layer thickness h:

$$\Omega\mathrm{Pr}A(\gamma)\,\frac{\cos(\alpha - \varphi)}{\cos\varphi}\exp\Big(-2(\xi'\cos\alpha + h(\xi')\sin\alpha - 1)^2$$

$$-\,\mathrm{Pe}\sin\alpha\Big(h - \frac{1}{6}\,\frac{ABh^3}{\cos\alpha + A(1 + Bh)h}\Big)\Big) - \frac{c_s^0\rho_s^0}{c_\mathrm{m}\rho_\mathrm{m}}\,\mathrm{Pe}\sin\alpha\int\limits_0^1 \nu(t)\,dt = \mathrm{Pe}\,\mathrm{Sf}\sin\alpha, \tag{33}$$

$$\gamma = \alpha - \varphi, \qquad \cos\varphi = 1\Big/\sqrt{1 + h'^2_{\xi'}}.$$

In the case of an infinitely small thickness of the liquid film ($h \approx 0$), we have $\varphi \approx 0$. From Eq. (33), in dimensional variables, we obtain

$$V_\mathrm{n} = 2WA(\alpha)\cos\alpha\exp\Big(-\frac{2x^2}{\omega_0^2}\Big)\Big/\Big[\pi\omega_0^2\Big(\rho_\mathrm{m}H_\mathrm{m} + c_s^0\rho_s^0(T_\mathrm{m} - T_0)\int\limits_0^1 \nu(t)\,dt\Big)\Big]. \tag{34}$$

Calculating the values of $h(\xi')$ and $\alpha(\xi')$ at each point ξ' from Eqs. (30) and (33), we obtain the solution of Eqs. (28)–(33). Figure 2 shows the dependences $H(\xi)$ and $\alpha(\xi)$ for different values of the cutting velocity V_c. The pressure in the gas holder is $P_0 = 0.5$ MPa, the plate thickness is $L = 0.5$ mm, the radiation power is $W = 600$ W, and the beam radius is $\omega_0 = 70$ μm. Figure 3 shows the distributions of the U and V components of the liquid-flow velocity along the coordinate η at the lower boundary of the cutting kerf for $\xi = L$, where the boundary-layer thickness is maximum. With increasing cutting velocity, the melt thickness and the flow-velocity components increase. Figure 4 shows the temperature distribution near the metal melting boundary. As the cutting velocity increases, the heating depth of the solid material decreases and becomes approximately equal to 100 μm for $V_\mathrm{c} \geqslant 160$ mm/sec.

Cutting-Front Surface. If we neglect the liquid thickness (according to Fig. 2a, it is several microns), then substituting V_n from Eq. (34) into the equation of kinematic compatibility (17), we can calculate the shape of the cutting surface $z = z_\mathrm{m}(x)$. In the dimensionless form, Eq. (17) contains one parameter σ:

$$\frac{\partial\beta_\mathrm{m}}{\partial t'} - \frac{\partial\beta_\mathrm{m}}{\partial x'} = -\sigma A(\alpha)\exp(-x'^2), \tag{35}$$

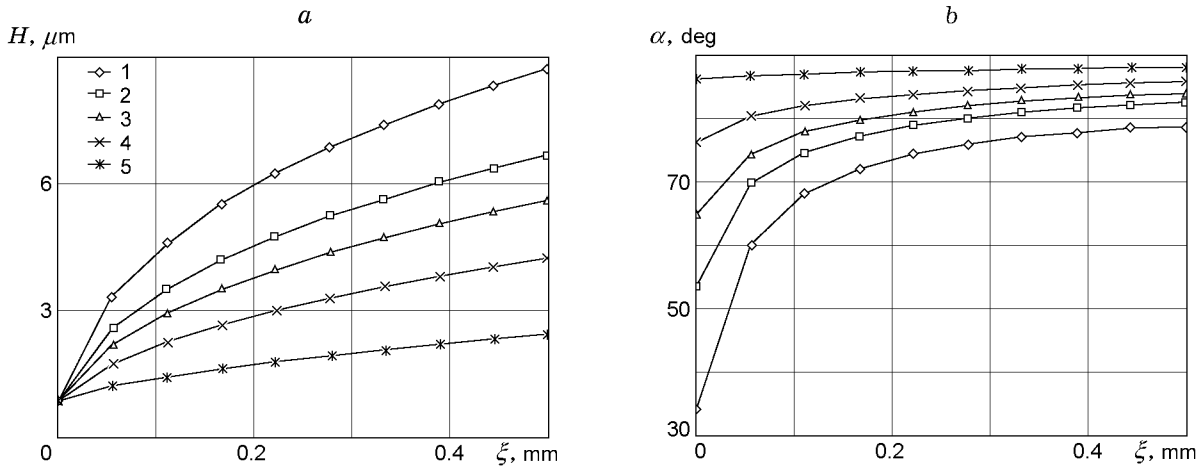

Fig. 2. Thickness of the boundary layer of the liquid $H(\xi)$ (a) and the angle $\alpha(\xi)$ (b) versus the cutting velocity $V_c = 500$ (1), 250 (2), 160 (3), 80 (4), and 20 mm/sec (5).

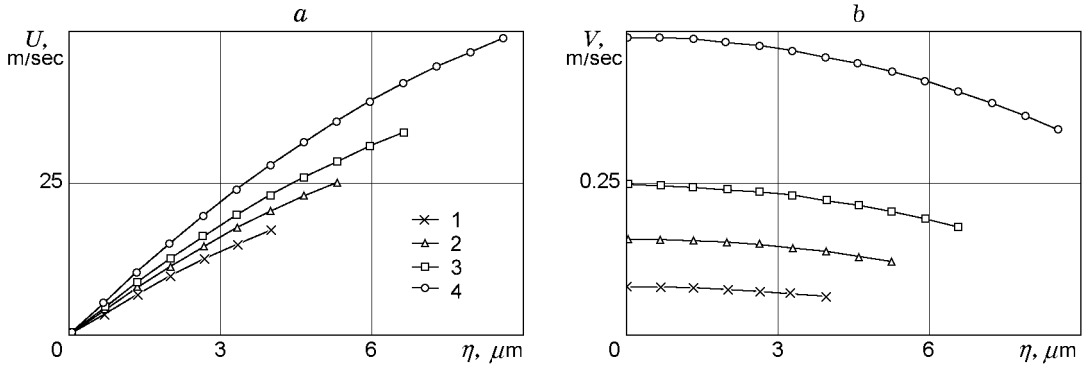

Fig. 3. Distribution of the liquid-velocity components $U(L,\eta)$ (a) and $V(L,\eta)$ (b) over the cutting depth for $V_c = 80$ (1), 160 (2), 250 (3), and 500 mm/sec (4).

where $x' = x/\omega_0$, $t' = tV_c/\omega_0$, $\beta_m = z_m/\omega_0$, $\cos\alpha = 1\Big/\sqrt{1+(\beta'_m)^2_{x'}}$, and

$$\sigma = \frac{2W}{\pi\omega_0^2 V_c\Big(\rho_m H_m + \rho_s^0 c_s^0 (T_m - T_0)\int\limits_0^1 \nu(t)\,dt\Big)}.$$

If the specific heat capacity and material density are independent of temperature ($c_s \equiv c_s^0$ and $\rho_s \equiv \rho_s^0$), we obtain $\int\limits_0^1 \nu(t)\,dt = 1$. Equation (35) with the initial condition $\beta_m(0,x') = 0$ is solved numerically by the pseudo-transient method in the region $x' \in [-\chi,\chi]$, where $\chi = L/\omega_0$. The calculated dependence of the maximum depth of the cutting kerf χ on the dimensionless parameter σ and also experimental data are shown in Fig. 5.

Sheets of low-carbon ($L = 1$, 2, and 3 mm) and electrotechnical ($L = 0.5$ mm) steels were used in experiments. The laser source was a flow-type CO_2 laser with a self-filtered resonator. The distribution of intensity of the laser beam is close to the Gaussian distribution. Cutting was performed by a beam with circular polarization. In cutting low-carbon steel, the beam was focused by a lens made of zinc selenide with a focal distance of 190 mm. Cutting of electrotechnical steel was performed using a two-lens objective optimized to reduce spherical aberration. Nitrogen was used as an assist gas. The limiting cutting velocity was determined in the experiments, the sheet thickness, radiation power, and pressure of the assist gas being varied. The main parameters of the process and the test results are listed in Table 2.

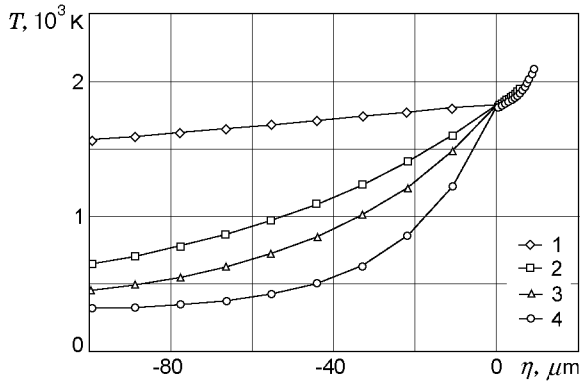

Fig. 4

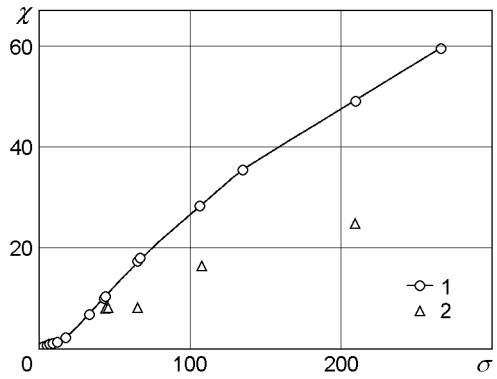

Fig. 5

Fig. 4. Temperature distribution in the liquid-melt layer and in the solid for $V_c = 20$ (1), 160 (2), 250 (3), and 500 mm/sec (4).

Fig. 5. Maximum depth of the cutting kerf χ versus the parameter σ: points 1 and 2 refer to the calculation and experiment, respectively.

TABLE 2

L, mm	W, W	P_0, atm	ω_0, μm	σ	V_c^{max}, mm/sec
0.5	337	10	60	43.5	134.0
0.5	427	10	60	44.0	167.0
0.5	517	10	60	44.4	200.0
1.0	1080	5	120	65.3	71.0
2.0	1080	5	120	107.0	43.4
3.0	1080	5	120	209.0	22.2

The analysis of the test results shows that the parameters χ and σ may be used to generalize the results of studying GLC regimes. A comparison of experimental data and the calculated dependence $\chi(\sigma)$ (Fig. 5) reveals their qualitative agreement, especially for moderately high values of the parameters χ and σ corresponding to low values of L and W. However, a difference arises with increasing L and W. The calculated value of the limiting cutting thickness L is greater than the experimental one, which may be caused by the following reasons.

1. A one-dimensional heat-conduction equation was solved in calculating heat losses, i.e., all radiation energy was spent on heating the substance in the cutting direction. In experiments, there are also heat losses to the side walls, perpendicular to the cutting kerf, and these losses should increase with increasing cutting thickness and decreasing cutting velocity V_c.

2. Calculation of GLC processes depends on a large number of parameters whose values are unknown. For example, insurmountable difficulties arise in the description of interaction of radiation and the melted metal surface. In experiments with a narrow and deep cutting kerf, multiple reflection of radiation from the side walls and melt surface occurs, and the shape of the latter is difficult to predict.

3. It is assumed in calculations that the material is removed as the melting point is reached; therefore, melt overheating is ignored.

4. Material evaporation is ignored in calculations; however, according to [10], the energy spent on evaporation and melting is comparable in magnitude.

Conclusions. Interaction of laser radiation and the material surface under conditions of GLC of the metal is studied theoretically and experimentally. A law of energy conservation on the cutting surface is derived, which takes into account the thickness of the liquid film of the melt. A numerical dependence is obtained, which is used to choose the optimal cutting conditions and radiation parameters. It is shown that the temperature dependence of thermophysical parameters of the metal should be taken into account.

The authors are grateful to V. I. Yakovlev for discussions and valuable comments on this work and also to S. A. Konstantinov for participation in experiments and assistance in interpreting the results.

REFERENCES

1. A. A. Vedenov and G. G. Gladush, *Physical Processes in Laser Processing of Materials* [in Russian], Énergoatomizdat, Moscow (1985).
2. J. Pawell, *CO_2 Laser Cutting*, Springer-Verlag (1993).
3. M. Vicanek, G. Simon, H. M. Urbassek, and I. Decker, "Hydrodynamical instability of melt flow in laser cutting," *J. Phys., D, Appl. Phys.*, **20**, 140–145 (1987).
4. N. K. Makashov, E. S. Asmolov, V. V. Blinkov, et al., "Gas dynamics of cutting metals by continuous laser radiation in an inert gas," *Kvant. Élektron.*, **19**, No. 9, 910–915 (1992).
5. S. Kaczmarek, J. Rafa, W. Przetakiewicz, and A. Pawlata, "Theoretical model of the steel sheets cutting with a CO_2–CW technological laser," *Optoelectronica*, **1**, No. 3, 7–16 (1993).
6. L. Cai and P. Sheng, "Analysis of laser evaporative and fusion cutting," *J. Manuf. Sci. Eng.*, **118**, 225–234 (1996).
7. P. Strömbeck and A. Kar, "Self-focusing and beam attenuation in laser materials processing," *J. Phys., D, Appl. Phys.*, **31**, 1438–1448 (1998).
8. K. Farooq and A. Kar, "Removal of laser-melted material with an assist gas," *J. Appl. Phys.*, **83**, No. 12, 7467–7473 (1998).
9. G. N. Abramovich, *Applied Gas Dynamics* [in Russian], Nauka, Moscow (1976).
10. E. Stuart and H. N. Rutt, "Selection criteria for polarizing mirrors for use in high-power CO_2-lasers," *J. Phys., D, Appl. Phys.*, **22**, 901–905 (1989).
11. G. Schlichting, *Boundary Layer Theory*, McGraw-Hill, New York (1968).
12. B. E. Neimark (ed.), *Physical Properties of Steels and Alloys Used in Power Engineering: Handbook* [in Russian], Énergiya, Moscow (1967).
13. V. S. Chirkin, *Thermophysical Properties of Materials in Nuclear Power Engineering* [in Russian], Atomizdat, Moscow (1968).
14. A. V. Nesterov and V. G. Niz'ev, "Special features of cutting metals by a laser beam with axisymmetric polarization," *Izv. Ross. Akad. Nauk, Ser. Fiz.*, **63**, No. 10, 2039–2046 (1999).
15. V. Semak and A. Matsunava, "The role of recoil pressure in energy balance during laser materials processing," *J. Phys., D, Appl. Phys.*, **30**, 2541–2552 (1997).